J Seismol
DOI 10.1007/s10950-007-9078-7

ORIGINAL ARTICLE

Constraints from precariously balanced rocks on preferred rupture directions for large earthquakes on the southern San Andreas Fault

Kim Olsen · James Brune

Received: 22 March 2007 / Accepted: 22 November 2007

Abstract We have compared near-fault ground motions from TeraShake simulations of M_w7.7 earthquake scenarios on the southern San Andreas Fault with precariously balanced rock locations. The TeraShake scenarios with different directions of rupture generate radically different ground motions to the northwest of the Los Angeles Basin, primarily because of directivity effects, and thus provide constraints on the ground motion and rupture direction for the latest (1690) large event on that section of the San Andreas Fault. Due to the large directional near-field ground motions predicted by the simulations, we expect the precariously balanced rocks to be located primarily in the backward rupture direction or near the epicenter. Preliminary results favor persistent nucleation at or slightly northwest of the San Gorgonia Pass fault zone for large earthquakes on the southern San Andreas Fault.

Keywords Finite-difference simulation · Long-period ground motion · Precariously balanced rocks · San Andreas Fault · Rupture directivity

K. Olsen (✉)
Dept of Geological Sciences, San Diego State University,
5500 Campanile Dr,
San Diego, CA 92182, USA
e-mail: kbolsen@sciences.sdsu.edu

J. Brune
Nevada Seismological Laboratory, University of Reno,
Reno, NV 89557, USA

1 Introduction

The two segments of the San Andreas Fault south of the 1906 rupture, the San Bernardino Mountains segment and the Coachella Valley segment, have not produced major earthquakes since 1812 and about 1690 (Weldon et al. 2004), respectively. The average recurrence interval for large events with surface rupture on these segments are 146+91–60 and 220± 13 years, respectively (Working Group on California Earthquake Probabilities 1995). To estimate the expected ground motions in southern California for such event, Olsen et al. (2006, 2008) simulated 4 min of 0–0.5-Hz wave propagation for M_w7.7 earthquake scenarios between Cajon Creek and Bombay Beach (see Fig. 1), the TeraShake simulations. The areal extent of the TeraShake simulations was a rectangular region, 600 km along N50W and 300 km along N40E (see Fig. 1). The simulations used a 3,000 by 1,500 by 400 mesh, or 1.8 billion cubes with dimensions 200 m^3. The three-dimensional crustal structure was a subset of the Southern California Earthquake Center (SCEC) Community Velocity Model (Magistrale et al. 2000) Version 3.0, with elastic parameters constrained by gravity and reflection seismic data, oil-company drill holes, and shallow geotechnical borings. The depth extent of the model is 80 km. The near-surface S-wave velocity was truncated at 500 m/s due to computational limitations. However, comparisons with finite element synthetics computed using very fine discretization of the low-velocity layers suggest

that the neglect of velocities below 500 m/s in the SCEC model causes at most a small underestimate of amplitudes in the 0–0.5-Hz band, typically less than about 10–20%. No surface topography was included in the simulations.

Two sets of simulations for large earthquakes on the southern San Andreas Fault were carried out, TeraShake-1 and TeraShake-2. For both sets of simulations, the San Andreas Fault geometry was approximated as five vertical, planar segments from the 2002 US Geological Survey (USGS) National Hazard Maps (Fig. 1). The rupture length is 200 km, and the down-dip width is 15 km. The TeraShake-1 simulations (Olsen et al. 2006) used a kinematic description of the source model based on that inferred for the 2002 M_w7.9 Denali earthquake (Oglesby et al. 2004). The source is modeled as a kinematic slip function with six 1-s time-windows of Brune pulses of 0.5-s rise time. This source model was found to produce 0.01–0.5-Hz synthetic seismograms in good agreement with observed strong motion data (Oglesby et al. 2004). The TeraShake-2 simulations (Olsen et al. 2008) used a more realistic mechanical (dynamic) description of the rupture propagation. A slip-weakening friction law with initial stress and slip-weakening distance inferred from dynamic models of the 1992 Landers, CA, USA earthquake (Peyrat et al. 2001) was used in the dynamic rupture propagation.

The TeraShake-1 (kinematic) and TeraShake-2 (dynamic) sources show important differences and similarities. The maximum slip and sliprate for both sets of rupture models reach about 10 m and 5 m/s, respectively. The kinematic source is characterized by relatively large, smooth asperities and a constant rupture velocity. The dynamic source is characterized by strong variations in rupture speed as well as frequent separation into several slipping areas of highly varying shape and sliprate. However, the average rupture velocity for the TeraShake-2 scenarios is close to the constant value of 3.3 km/s used for TeraShake-1, generating a rupture duration of approximately 70 s for both sets of rupture models. The duration of slip (at a given point) is similar in the kinematic and dynamic models, although much more variable in the latter model.

Simulations were carried out for kinematic and dynamic sources initiating at the northwestern end rupturing toward the southeast (NW–SE; TS1.2,

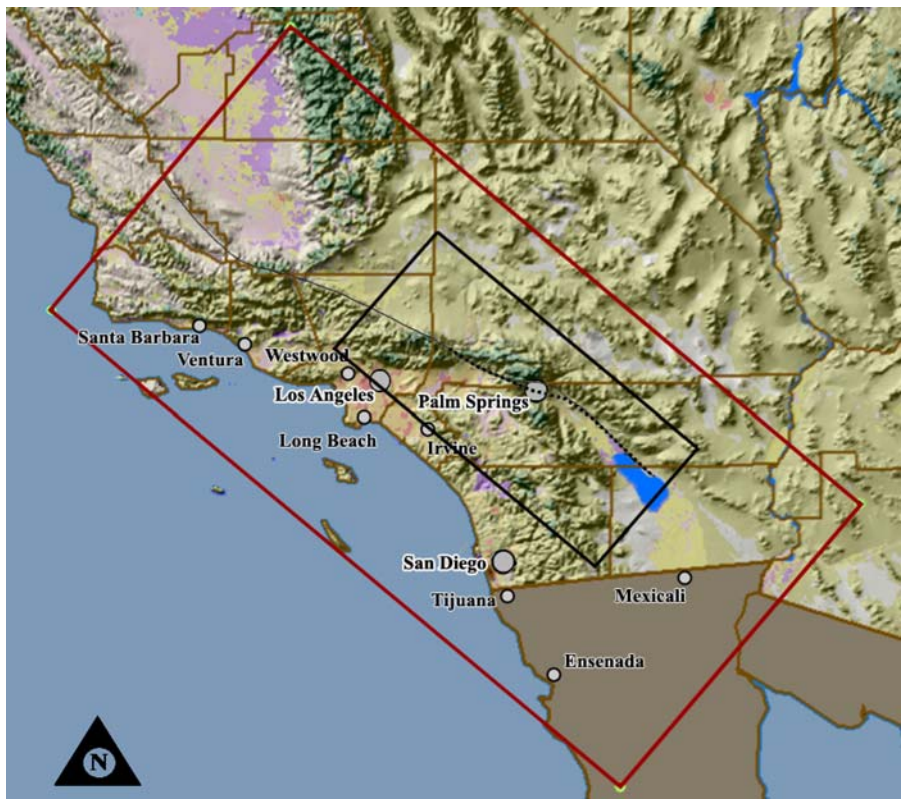

Fig. 1 Location map for the TeraShake simulations. The *red rectangle* depicts the simulations area, which is rotated 40° clockwise from North. The *black rectangle* depicts the area used for comparison of PGVs and locations of PBRs. The *dotted line* depicts the part of the San Andreas Fault that ruptured in the TeraShake simulations

TS2.3), starting at the southeastern end and rupturing toward the northwest (SE–NW; TS1.3–4, TS2.1–2) and for a bilateral rupture (TS1.5) with kinematic source. The peak ground velocity (PGV) distributions for both TeraShake-1 and TeraShake-2 simulations reveal a striking contrast in ground motion pattern between NW–SE versus SE–NW rupture scenarios. The ground motion is focused in the direction of rupture, and this rupture directivity effect is dramatically modified by interactions with the chain of sedimentary basins (the San Bernardino, Chino, San Gabriel, and Los Angeles basins) running westward from the northern terminus of the rupture to downtown Los Angeles. This chain of basins forms a low-velocity structure that acts as a waveguide, trapping seismic energy along the southern edge of the San Bernardino and San Gabriel Mountains and channeling it into the Los Angeles region. This guided wave is efficiently excited by the SE–NW rupture scenarios, but not appreciably by the NW–SE rupture scenarios. In contrast, the NW–SE scenarios would generate PGVs of about an order of magnitude smaller in the Los Angeles basin, but strong reverberations for an extended duration at locations inside the Salton Trough, including the Coachella and Imperial Valleys (Olsen et al. 2006, 2008).

While the TeraShake-1 and TeraShake-2 simulations produce similar spatial patterns of ground motion, the dynamic sources decrease the maximum ground motions obtained by the kinematic source, in some areas of Los Angeles by factors of 2–3. The primary reason for the smaller ground motions is a more incoherent wavefield radiated from the complex dynamic source. This complexity consists mainly of abrupt changes in rupture speed and direction, which produces characteristic ‘sun burst’ patterns of elevated ground motions along bands extending outward from the fault (Olsen et al. 2008).

The TeraShake simulations were carried out using a 4th-order staggered-grid finite difference code (Olsen 1994) with a coarse-grained implementation of the memory variables for a constant-Q solid (Day and Bradley 2001) and Q relations were validated against data (Olsen et al. 2003). The dynamic rupture propagation used in the TeraShake-2 simulations was implemented using the stress-glut method (Andrews 1999). We use the efficient Perfectly Matched Layers absorbing boundary conditions on the sides and bottom of the model (Marcinkovich and Olsen 2003).

2 Correlation of precariously balanced rocks and TeraShake PGVs

In lack of strong ground motion recordings, the location of granitic precariously balanced rocks (PBRs) have been used to estimate upper bounds of the seismic shaking for periods sufficiently long to sample an earthquake rupture forecast (Bell et al. 2004; Purvance 2005; Purvance et al. 2005). PBRs are mapped near the section of the southern San Andreas Fault that ruptured in the TeraShake simulations (see Fig. 2) by James Brune and colleagues.

Here, we use the PBRs to establish bounds on the intensity of shaking and compare to the PGV (here defined as the root sum of squares of all three components) patterns from TeraShake simulations with different rupture directions and source descriptions. A comparison of the locations of PBRs with TeraShake-1 and TeraShake-2 PGV distributions are shown in Figs. 3 and 4, with the 50-cm and 35-cm PGV contours superimposed for the TeraShake-1 and TeraShake-2 results, respectively. The relatively smaller reference PGV for TeraShake-2 is due to the smaller ground motions generated from the more complex dynamic sources, as discussed above. The PGV contours are somewhat arbitrarily selected

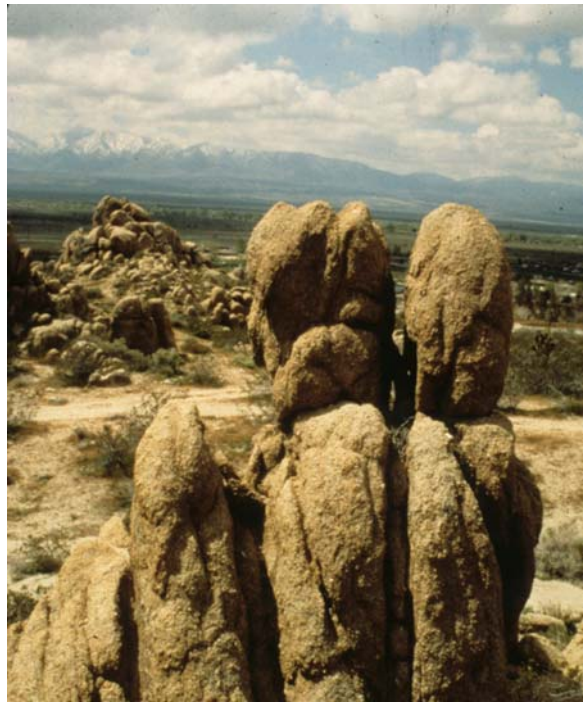

Fig. 2 Precariously balanced rocks at Lovejoy Buttes

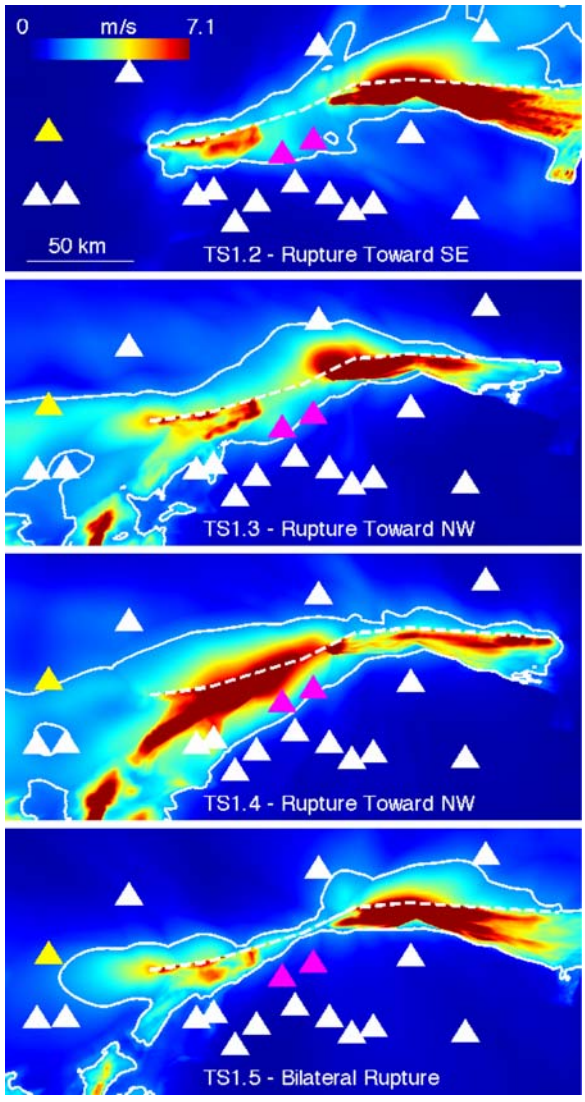

Fig. 3 PGV distributions from four TeraShake-1 simulations (TS1.2–5). The *dashed line* is the section of the San Andreas Fault that ruptured in the simulations. The *solid line* is the 50-cm/s PGV contour. The *triangles* depict precarious rock locations, with sites at Banning and Beaumont in *magenta* and Lovejoy Buttes in *yellow*

because peak ground accelerations (PGAs) are required to determine absolute toppling thresholds for the PBRs. However, the shape of the PGV contours may provide guidance to a preferred rupture direction on the southern San Andreas Fault. Note the characteristic cone-shaped pattern for the PGVs, with a relatively narrow width along the fault around the epicenter and widening along the fault away from the epicenter. Several PBRs are located at sites experiencing ~50 cm/s or higher PGV for the TeraShake-1 scenarios with rupture starting either at the NW or SE end of the fault segment (Fig. 3, TS1.2–4). In particular, the two PBRs with the smallest distance to the segments of the San Andreas Fault used in the TeraShake simulations, located near Banning and Beaumont, may provide important clues to a preferred rupture direction of the fault. These two PBRs tend to experience consistently large PGVs for unilateral rupture scenarios but much smaller PGVs for a simulation with bilateral rupture with nucleation near these two sites (TS1.5, see Fig. 3). Thus, the correlation of PBRs with TeraShake-1 PGVs for the available simulations tends to favor bilateral over unilateral rupture directions on the southern San Andreas Fault from the TeraShake-1 simulations.

The correlation of PBRs with PGVs from TeraShake-2 simulations (Fig. 4) provides less guidance for the rupture direction, in part due to the lack of a

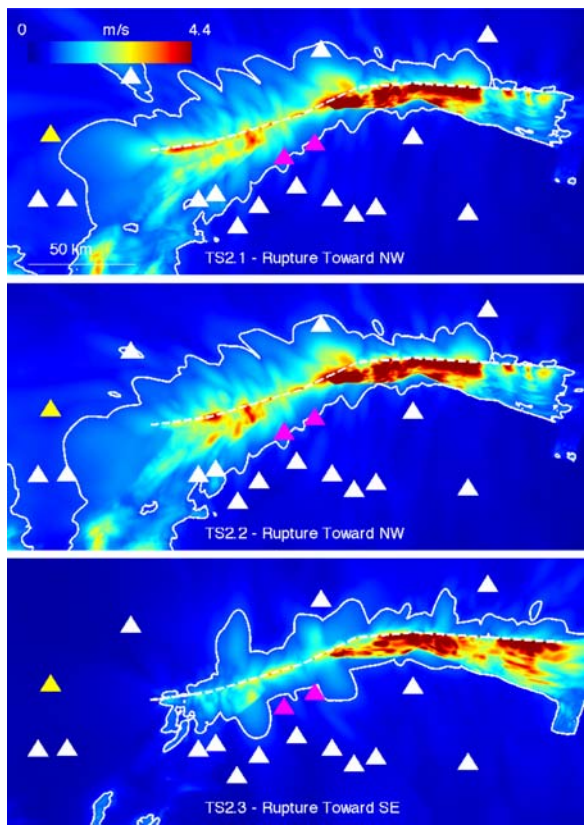

Fig. 4 PGV distributions from four TeraShake-2 simulations (TS2.1–3). The *dashed line* is the section of the San Andreas Fault that ruptured in the simulations. The *solid line* is the 35-cm/s PGV contour. The *triangles* depict precarious rock locations, with sites at Banning and Beaumont in *magenta* and Lovejoy Buttes in *yellow*

bilateral rupture scenario with dynamic source description. In addition, the stronger local variation of the PGVs for TeraShake-2 due to the larger complexity of the dynamic sources complicates the correlation with the PBRs. However, similar cone-shaped PGV patterns as noted for the TeraShake-1 simulations prevail for the dynamic sources. The TS2.3 simulation (rupture toward the SE) generates, on average, a narrower cone of PGVs expanding in the rupture direction for a M_w7.7 event occurring on this part of the San Andreas Fault, with all mapped PBRs experiencing PGVs less than 35 cm/s. In contrast, several PBRs are located inside or near (including those at Banning and Beaumont) the 35-cm/s contour for TS2.1–2 (rupture toward the NW). Thus, the TeraShake-2 results tend to favor a NW–SE rupture direction over a SE–NW rupture direction.

3 Discussion and conclusions

We have used comparison of near-fault ground motions from four TeraShake-1 and three TeraShake-2 scenario earthquake simulations with PBR locations to constrain the preferred rupture direction of the southern San Andreas Fault. The observed PBRs closest to the segments of the San Andreas Fault rupturing in the TeraShake simulations are located near Banning and Beaumont, approximately 1/3 of the distance from the NW end to the SE end of the rupturing fault. The presence of the two near-fault PBRs suggests that large earthquakes on the southern San Andreas consistently generate lower strong ground motions along the fault in this area. Analysis of near-fault rupture patterns for the TeraShake simulations suggests that the epicentral area generally experiences smaller PGVs as compared to sites along the fault in the rupture direction. This observation is consistent with the effects of rupture directivity for large, shallow-crustal earthquakes on near-vertical faults. Furthermore, the seven TeraShake simulations cover a realistic range of maximum slip and sliprates, including the part of the fault near the Banning and Beaumont PBRs (see Fig. 5). Thus, any bias from the rupture models affecting the correlation of PGVs and PBRs is likely limited. We conclude that the distribution of PBRs is consistent with persistent nucleation of large earthquakes on the southern San Andreas Fault near Palm Springs (see Fig. 1). The PGVs for the bilateral rupture scenario TS1.5, with epicenter close to the Banning and Beaumont PBRs, and the NW–SE rupture scenario TS2.3, produce the best correlation with the location of near-fault PBRs. Two different possibilities for a preferred rupture direction, both with nucleation toward the north–central or northern part of the causative fault in the TeraShake scenarios, are consistent with the results: (1) that successive ruptures on the southern San Andreas have propagated both directions, or (2) that the ruptures propagate bilaterally.

The geometry of the San Andreas Fault shows increased complexity in the proposed area of persistent nucleation. The San Andreas Fault is divided into two sub-parallel traces, the Mission Creek fault and the Banning fault near this area. Here, the NW–SE strike of the San Andreas Fault to the NW and SE is replaced by a WNW–ESE strike in the San Gorgonio fault zone. The M_w6.1 1986 North Palm Springs and 1948 M_L6.3 Desert Hot Springs earthquakes occurred in this area, with epicenters between the surface traces of the Banning and Mission Creek faults. The focal mechanisms for both events occurred on NE-dipping faults with a thrust component (e.g., Nicholson 1996), in agreement with the significant vertical relief of the mountains in this area. The stress conditions required for nucleation of an earthquake depends on the geometry of the fault (e.g., King et al. 1994), and it is possible that the regional stress accumulation may be more favorable for nucleation on a dipping fault rather than a near-vertical fault geometry (as used for the model for the San Andreas Fault in this study). An example of such scenario was the 2002 M_w7.9 Denali, AK, USA earthquake, which was initiated by a thrust earthquake at one end. Moreover, Freed and Lin (2002) showed that the nearby 1992 M_w7.3 Landers and 1999 M_w7.1 Hector Mine earthquakes brought the San Andreas Fault closer to failure in the San Gorgonio Pass area. Finally, it should be noted that the concentration of PBRs near Banning and Beaumont might be explained by reduced ground motions on the footwall of San Gorgonio Pass fault zone, due to the hanging wall effect (Abrahamson and Somerville 1996).

The TeraShake simulations currently only contain frequencies less than 0.5 Hz, while near-fault peak motions oftentimes occur at frequencies larger than 0.5 Hz. Thus, near-fault peak ground motions estimated from the simulations, in particular PGAs

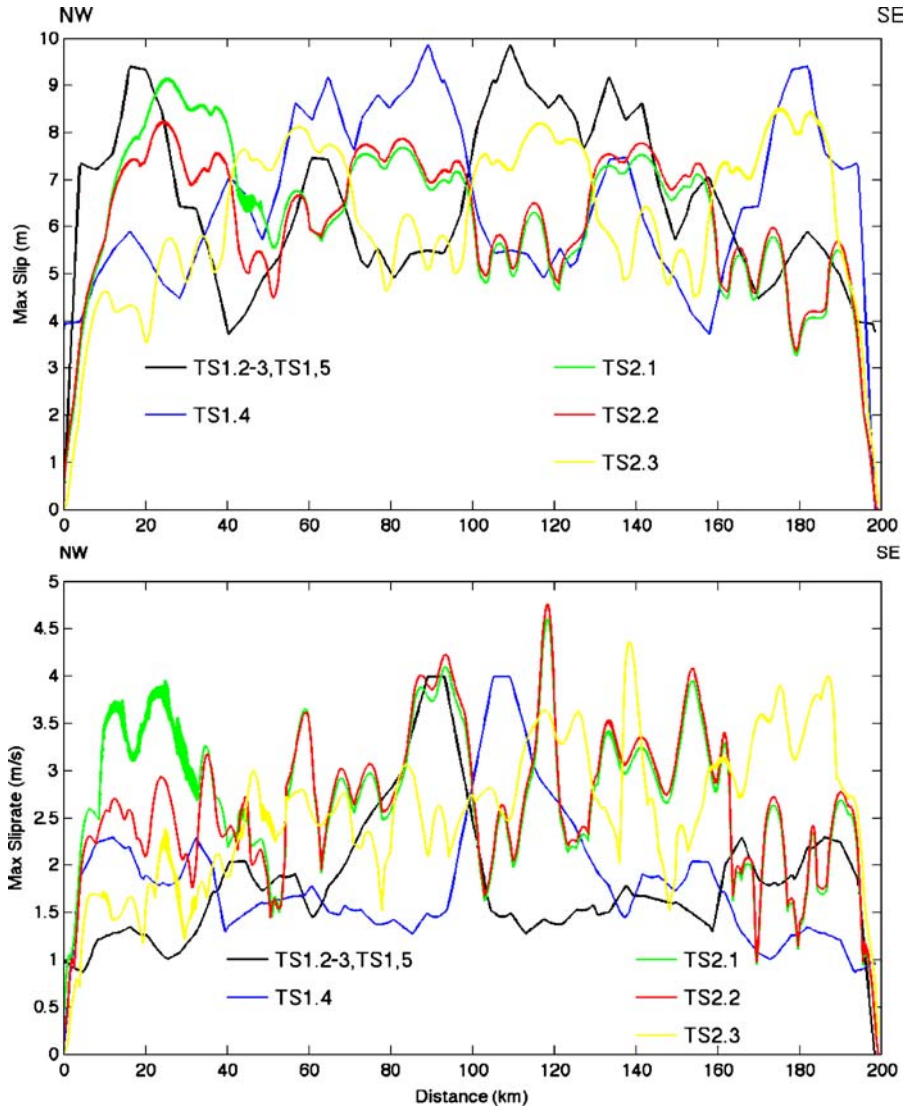

Fig. 5 (*top*) Maximum slip and (*bottom*) maximum sliprate for the TeraShake simulations from the NW (*left*) to the SE (*right*) end of the segments of the San Andreas fault rupturing in the TeraShake simulations (*dotted line* in Fig. 1)

required to determine the toppling threshold for the PBRs, are likely underestimated. Future efforts should therefore work toward increasing the maximum frequency of the synthetic seismograms for the southern San Andreas scenarios. Due to computational limitations, the largest frequency for deterministic ground motion models is currently limited to 1–2 Hz, when realistic near-surface velocities are included (see, for example, Benites and Olsen 2005). Instead, several recent methods have been proposed to generate realizations of broadband synthetic seismograms using hybrid techniques, combining deterministic long-period synthetics and shorter-period stochastic synthetics (e.g., Mai and Olsen 2006; Graves and Pitarka 2004; Liu et al. 2006). These methods are computationally relatively inexpensive and allow for the generation of synthetics with frequencies up to 10 Hz or higher. Using these techniques, a range of PGA estimates at the PBR locations can be found from an ensemble of realizations of broadband synthetics.

Acknowledgements This project is funded by National Science Foundation (NSF) Information Technology Research through the award Division of Earth Sciences (EAR)-0122464 (The SCEC Community Modeling Environment: An Information Infrastructure for System-Level Earthquake Research). SCEC is funded by NSF Cooperative Agreement EAR-0106924 and USGS Cooperative Agreement 02HQAG0008. This is SCEC publication #1143.

References

Abrahamson NA, Somerville PG (1996) Effects of the hanging wall and footwall on ground motions recorded during the Northridge earthquake. Bull Seis Soc Am 86:593–599

Andrews JD (1999) Test of two methods for faulting in finite-difference calculations. Bull Seis Soc Am 89:931–937

Bell JW, Brune JN, Zeng Y (2004) Methodology for obtaining constraints of ground motion from precariously balanced rocks. Bull Seis Soc Am 94:285–303

Benites R, Olsen KB (2005) Modeling strong ground motion in the Wellington Metropolitan area, New Zealand. Bull Seis Soc Am 95:2180–2196

Day SM, Bradley CR (2001) Memory-efficient simulation of anelastic wave propagation. Bull Seism Soc Am 91:520–531

Freed AM, Lin J (2002) Accelerated stress buildup on the southern San Andreas Fault and surrounding regions caused by Mojave Desert earthquakes. Geology 30:571–574

Graves RW and Pitarka A (2004) Broadband time history simulation using a hybrid approach. Proceedings of the 13th World Conference on Earthquake Engineering, Vancouver, Canada, August 1–6, 2004, Paper No. 1098.

King G, Stein R, Lin J (1994) Static stress changes and the triggering of earthquakes. Bull Seis Soc Am 84:935–953

Liu P-C, Archuleta RJ, Hartzell SH (2006) Prediction of broadband ground-motion time histories: hybrid low/high-frequency method with correlated random source parameters. Bull Seis Soc Am 96:2118–2130

Mai PM, Olsen KB (2006) Near-field broadband ground motions based on low-frequency finite-difference synthetics merged with high-frequency scattering operators. Seis Res Lett 77:300

Magistrale H, Day SM, Clayton R, Graves RW (2000) The SCEC southern California reference three-dimensional seismic velocity model version 2. Bull Seis Soc Am 90 (6B):S65–S76

Marcinkovich C, Olsen KB (2003) On the implementation of perfectly matched layers in a 3D fourth-order velocity-stress finite-difference scheme. J Geophys Res 108(B5):2276

Nicholson C (1996) Seismic behavior of the southern San Andreas Fault zone in the Coachella Valley, California: comparison of the 1948 and 1986 earthquake sequences. Bull Seis Soc Am 86:1331–1349

Oglesby DD, Dreger DS, Harris R, Ratchkovski N, Hansen R (2004) Inverse kinematic and forward dynamic models of the 2002 Denali, Alaska earthquake. Bull Seis Soc Am B6:S214–S233

Olsen KB (1994) Simulation of three-dimensional wave propagation in the Salt Lake Basin, *Ph.D. Thesis*, University of Utah, Salt Lake City, Utah, 157 pp

Olsen KB, Day SM, Bradley CR (2003) Estimation of Q for long-period (>2 s) waves in the Los Angeles Basin. Bull Seis SocAm 93:627–638

Olsen KB, Day SM, Minster JB, Cui Y, Chourasia A, Faerman M, Moore R, Maechling P, Jordan T (2006) Strong shaking in Los Angeles expected from southern San Andreas earthquake. Geophys Res Lett 33:L07305 DOI 10.1029/2002JB002235

Olsen KB, Day SM, Minster JB, Cui Y, Chourasia A, Okaya D, Maechling P and Jordan T (2008) Spontaneous rupture simulations of Mw7.7 earthquakes on the southern San Andreas fault. Bull Seis Soc Am (in press)

Peyrat S, Olsen KB, Madariaga R (2001) Dynamic modeling of the 1992 Landers earthquake. J Geophys Res 106:26,467–26,482

Purvance MD (2005) Overturning of slender blocks: numerical investigation and application to precariously balanced rocks in southern California, PhD Dissertation, University of Nevada, Reno

Purvance MD, Brune JN, and Anooshehpoor A (2005) Attenuation relation consistency with precariously balanced rocks, Proceedings 2005 SCEC Conferenece, Palm Springs, CA, Sept. 11–14.

Weldon R, Scharer K, Fumal T, Biasi G (2004) Wrightwood and the earthquake cycle: what a long recurrence record tells us about how faults work. Geol Seis Am 14:4–10

Working Group on California Earthquake Probabilities Seismic hazards in southern California: probable earthquakes, 1994 to 2024, 1995. Bull Seis Soc Am 85:379–439